

1 Synergistic substrate cofeeding stimulates reductive metabolism

2
3 Junyoung O. Park^{1†}, Nian Liu^{1†}, Kara M. Holinski¹, David F. Emerson¹, Kangjian Qiao¹, Benjamin M.
4 Woolston¹, Jingyang Xu¹, Zbigniew Lazar^{1,2}, M. Ahsanul Islam¹, Charles Vidoudez³, Peter R. Girguis³,
5 and Gregory Stephanopoulos^{1*}

6
7 ¹ Department of Chemical Engineering, Massachusetts Institute of Technology, 77 Massachusetts
8 Avenue, Cambridge, MA 02139

9 ² Department of Biotechnology and Food Microbiology, Wroclaw University of Environmental and
10 Life Sciences, Chelmonskiego 37, 51-630, Wroclaw, Poland

11 ³ Department of Organismic and Evolutionary Biology, Harvard University, 16 Divinity Avenue,
12 Cambridge, MA 02138

13 † Equal contribution

14 * Correspondence to G.S.: gregstep@mit.edu

15
16 Advanced bioproduct synthesis via reductive metabolism requires coordinating carbons, ATP, and
17 reducing agents, which are generated with varying efficiencies depending on metabolic pathways.
18 Substrate mixtures with shortcut access concurrently to multiple pathways may optimally satisfy
19 these biosynthetic requirements. However, native regulation favoring preferential utilization
20 precludes cells from co-metabolizing multiple substrates. Here we explore mixed substrate
21 metabolism and tailor pathway usage to synergistically stimulate carbon reduction. By controlled
22 cofeeding of superior ATP- and NADPH-generators as “dopant” substrates to cells primarily
23 utilizing inferior substrates, we circumvent catabolite repression and drive synergy in two
24 divergent organisms. Glucose doping in *Moorella thermoacetica* stimulates CO₂ reduction (2.3
25 g/g_{cell}/hr) into acetate by augmenting ATP synthesis via pyruvate kinase. Gluconate doping in
26 *Yarrowia lipolytica* accelerates acetate-driven lipogenesis (0.046 g/g_{cell}/hr) by obligatory NADPH
27 synthesis through the pentose cycle. Together, synergistic cofeeding produces CO₂-derived lipids
28 with 38% energetic efficiency and demonstrates potential to convert CO₂ into advanced
29 bioproducts.

31 Introduction

32 One of the greatest feats of metabolism is the ability to synthesize reduced compounds from input
33 substrates with varying oxidation states. Using reductive metabolism, cells reassemble the output
34 of substrate catabolism for energy-dense bioproduct synthesis¹. This process is often implemented
35 in both laboratory and industry with single organic carbon sources (e.g., sugars) as inputs due to
36 simplicity^{2,3}. Nonetheless, single substrates naturally impose stoichiometric constraints on
37 available carbons, energy, and redox cofactors, leading to biosynthetic imbalance and suboptimal
38 product yield. Thus, genetic rewiring of metabolic pathways is required to advantageously shift
39 these stoichiometries⁴, which precludes wide application of non-model organisms that lack suitable
40 genetic tools⁵.

41 Substrate mixtures, on the other hand, present the potential to alleviate such stoichiometric
42 constraints in reductive metabolism without genetic rewiring. Since each substrate has unique
43 efficiencies for carbon, energy, and cofactor generation, varying the relative amounts of substrates
44 in the mixture allows fine-tuning of carbon-to-energy-to-cofactor ratios. Furthermore, substrates
45 with different entry points to metabolism alleviate protein burdens by providing the required
46 components in fewer enzymatic steps. Nevertheless, mixed substrate metabolism is epitomized by
47 sequential (e.g., diauxie) and hierarchical (yet simultaneous) utilization based on substrate
48 preference⁶⁻⁸, reflecting the evolutionary fitness of cells in their native environments⁹. Despite the
49 recent success of substrate mixture batch fermentation using limited substrate pairs (that do not
50 trigger catabolite repression)^{10,11}, genetic engineering^{12,13}, and directed evolution¹⁴⁻¹⁶, the full
51 mixture spectrum remains inaccessible and thus unexplored.

52 Here we report a simple and universal solution to overcoming undesirable substrate preferences
53 and improving carbon reduction in various organisms. We eliminate catabolite repression by
54 controlling the continuous feed rate of preferred superior substrates to maintain negligible
55 concentrations in systems dominated by inferior substrates. Using this method, we explored mixed
56 substrate metabolism and therein observed enhanced metabolic productivity that exceeds the sum
57 of individual-substrate productivities.

58 This substrate cofeeding scheme was applied to two widely divergent organisms to optimize
59 reductive metabolism of lipogenesis and acetogenesis. We cultured the oleaginous yeast *Y. lipolytica*
60 on acetate and continuously fed limiting quantities of glucose, fructose, glycerol, or gluconate as
61 “dopant substrates” to augment reductive metabolism. In this fed-batch setup, cells simultaneously
62 consumed acetate and the supplemented substrate with acetate remaining as the primary carbon
63 source. In particular, the rate of lipogenesis with gluconate doping was twice as fast as that of the
64 acetate-only control. Tracing ¹³C from gluconate revealed that obligatory NADPH synthesis by
65 recursive use of the oxidative pentose phosphate pathway (oxPPP) was responsible for the
66 observed synergy with acetate.

67 We then set out to source acetate via acetogenesis, a reductive metabolic process starting from CO₂.
68 Acetogenic bacterium *M. thermoacetica* simultaneously consumes CO₂ and glucose with the latter
69 providing both ATP and electrons (e⁻) necessary for CO₂ fixation, cell maintenance, and growth¹⁷.
70 However, tracing ¹³C-labeled glucose revealed that glucose metabolism dominated and e⁻
71 generation was coupled to undesirable decarboxylation. To shift cellular metabolism towards

72 greater CO₂ incorporation, we designed a chemostat that continuously supplied limiting glucose
73 and ample H₂. Under these conditions, CO₂ reduction metabolism dominated, glucose primarily
74 produced ATP sufficient for cell maintenance via pyruvate kinase, and carbon-free e⁻ for net CO₂
75 reduction was supplied by H₂. Importantly, with dopant substrate glucose, *M. thermoacetica* rapidly
76 converted CO₂ into acetate exclusively, serving as the ideal input for gluconate-doped lipogenesis.

77 With the aforementioned synergy, we fixed CO₂ at 2.3 g per g cell dry weight per hour (g gCDW⁻¹ hr⁻¹)
78 1), substantially faster than ~0.05 g gCDW⁻¹ hr⁻¹ of typical photosynthetic systems¹⁸. Using the
79 resulting acetate, we produced lipids at 0.046 g gCDW⁻¹ hr⁻¹, a more than two-fold improvement
80 over the previously optimized system (~0.02 g gCDW⁻¹ hr⁻¹)¹⁹. Coordinating the glucose-doped
81 acetogenesis and gluconate-doped lipogenesis, we converted carbons in the most oxidized,
82 undesirable state (CO₂) to the reduced, energy-dense state (lipids) with 38% energetic efficiency.
83 Through substrate cofeeding, we overcame the limitation of ATP- and NADPH-dependent biological
84 carbon reduction, paving the path for CO₂-derived advanced bioproduct synthesis.

85 **Accelerating lipogenesis from acetate by enhancing NADPH generation in *Y. lipolytica***

86 Lipogenesis requires a balanced supply of acetyl-CoA, ATP, and NADPH at a ~1:1:2 ratio. Single
87 substrates, such as glucose and acetate, can provide all three building blocks for lipids¹⁹⁻²¹.
88 However, lipid synthesis from acetate, despite acetate's direct contribution to acetyl-CoA and ATP,
89 is slower compared to that from glucose²² (**Fig. 1A**). This is because in *Y. lipolytica*, NADPH
90 generation is mainly through oxPPP, which takes a series of ATP-intensive reactions to arrive at
91 starting from acetate²³.

92 We aimed to enhance acetate-to-lipid conversion by better supplying NADPH. Since glucose can
93 flow more directly into oxPPP than acetate, we provided both acetate and glucose to a *Y. lipolytica*
94 batch culture. Consistent with the widely accepted phenomenon of catabolite repression²⁴, cells
95 consumed glucose only at first (**Supplementary Fig. 1**). To overcome this selective preference (i.e.,
96 diauxie), we devised a fed-batch system, in which the same amount of glucose was instead
97 continuously supplied over the course of fermentation to an acetate culture (**Fig. 1B**). The feed rate
98 was kept slow to maintain negligible glucose concentrations in the reactor. In this setup, despite
99 constant introduction of glucose, we observed steadily decreasing acetate and no glucose in the
100 reactor, suggesting simultaneous consumption of the two carbon sources (**Fig. 1C**). Furthermore,
101 the fed-batch cofeeding strategy enhanced both the growth and lipid production in *Y. lipolytica*
102 significantly compared to the acetate-only control (**Fig. 1D,E**).

103 Using the same fed-batch system, we also tested supplementing other substrates (fructose, glycerol,
104 and gluconate) that enter metabolism near oxPPP as metabolic “dopants” to provide NADPH (**Fig.**
105 **2A**). In all cases, we observed simultaneous consumption of acetate and the supplemented
106 substrate (**Supplementary Fig. 2**). As with glucose, cell growth and lipid production were
107 enhanced (**Supplementary Fig. 3**) despite the supplemental substrates constituting only small
108 fractions of carbons (**Fig. 2B**). To distinguish whether the increase in lipid production was due to
109 cellular metabolism enhancements or simply having more cells in the culture, we determined
110 specific growth rates and productivities. Substrate doping nearly doubled both the specific growth
111 rate (**Fig. 2C**) and the specific lipid productivity during nitrogen-replete growth phase (**Fig. 2D**). In
112 nitrogen-depleted lipogenic phase, glucose, fructose, and glycerol cofeeding only modestly

113 enhanced specific productivity while gluconate cofeeding significantly outperformed all other
114 conditions (**Fig. 2E**).

115 **Recursive NADPH generation via the pentose cycle**

116 To understand the mechanism of accelerated lipid production, we aimed to elucidate how
117 continuous gluconate supplementation rewires metabolism. Tracing the carbons from [U-
118 ¹³C₆]gluconate by liquid chromatography-mass spectrometry (LC-MS), we observed that the ¹³C
119 atoms were confined to the PPP and upper glycolysis (**Fig. 3A and Supplementary Table 1**).
120 Gluconate enters metabolism as 6-phosphogluconate (6PG), which can only go in the oxidative
121 direction through oxPPP because the combined thermodynamics of glucose-6-phosphate
122 dehydrogenase and 6-phosphogluconolactonase ($\Delta G^{\circ} = -29$ kJ/mol) strongly favors the flow of 6PG
123 further into PPP²⁵. This causes gluconate to obligatorily generate NADPH via 6PG dehydrogenase,
124 which is likely responsible for the acceleration of lipogenesis. On the other hand, metabolites in the
125 TCA cycle as well as fatty acids were completely unlabeled, indicating exclusive contribution of
126 lipogenic acetyl-CoA and ATP from acetate (**Fig. 3A and Supplementary Table 1**). These labeling
127 data suggested the partitioned usage of metabolism where acetate primarily provided acetyl-CoA
128 and ATP while gluconate primarily provided NADPH to meet the metabolic demands of lipogenesis.

129 To further validate the hypothesis that gluconate enhances lipogenesis through NADPH
130 supplementation, we performed metabolic flux analysis using the labeling data, substrate uptake
131 rates, and lipid production rate. The flux distribution that best fit all these measurements revealed a
132 strong flux through the oxPPP NADPH-generating steps (**Fig. 3B and Supplementary Table 2**).
133 Interestingly, phosphoglucose isomerase operated in the reverse direction converting fructose-6-
134 phosphate (F6P) to glucose-6-phosphate (G6P). The flux analysis also revealed that gluconeogenic,
135 oxPPP, and non-oxPPP fluxes together form a metabolic cycle, which we termed the “pentose cycle”
136 (**Fig. 3B and Supplementary Table 2**). Akin to the TCA cycle, the pentose cycle recursively
137 oxidized the carbons from gluconate into CO₂ while preserving the electrons as NADPH for
138 lipogenesis, maximizing the dopant substrate’s role as a NADPH provider.

139 **Preferential use of glucose leads to excessive decarboxylation in CO₂-fixing *M. thermoacetica***

140 Acetogenesis is a reductive metabolic process that produces acetate from CO₂. In acetogenic
141 organisms, the reductive acetyl-CoA pathway incorporates CO₂ as carbonyl and methyl components
142 of the acetyl group²⁶ (**Fig. 4A**). The methyl branch of this pathway requires ATP, which acetogens
143 may recover by acetate production. This ATP conservation contributes to efficient autotrophic CO₂
144 fixation²⁷, but autotrophic culture conditions, which derive energy solely from inorganic sources
145 (e.g., oxidation of H₂), results in slow metabolism and low culture density^{28,29}.

146 Since glycolysis effectively produces ATP and e⁻ necessary for operating the reductive acetyl-CoA
147 pathway, we co-fed CO₂ and [U-¹³C₆]glucose to *M. thermoacetica* and looked for signs of CO₂
148 incorporation. If acetate were the only product, we would expect up to 100% carbon yield, that is,
149 three acetate molecules per glucose²⁹. On the other hand, with potential other products (e.g.,
150 pyruvate) or biomass components (e.g., Ser/Gly, Asp, and Glu), net CO₂ utilization becomes feasible
151 as some pathways generate reducing agents without CO₂ production or fix more CO₂ than the
152 amount produced (**Supplementary Fig. 4**). Since net CO₂ utilization depends on the types and

153 fractions of fermentation products, we quantified the cell growth, the secreted molecules, and their
154 carbon yields relative to glucose consumption (**Fig. 4B**). We observed the activity of the reductive
155 acetyl-CoA pathway as the produced acetate accounted for 77% of glucose carbons, exceeding what
156 is possible via glycolysis (67%). However, as glucose carbon consumption rate approximately
157 matched the total carbon output rate of major products (i.e., biomass, acetate, and formate
158 accounted for 93%), we did not observe net CO₂ utilization.

159 We hypothesized that our observed carbon yield was due to insufficient reducing agents available
160 for new CO₂ utilization and cells preferentially consuming glucose over CO₂. To trace the fate of ¹³C-
161 glucose carbons and to visualize metabolic pathway usage, we measured ¹³C enrichment in cellular
162 metabolites using LC-MS. Unlabeled CO₂ was provided in the headspace and CO₂ remained mostly
163 unlabeled (**Supplementary Fig. 5**). The carbons of glycolytic intermediates were ≥90% labeled
164 except for pyruvate, which was ~50% labeled (**Fig. 4C, Supplementary Table 3**). The lower
165 labeling in pyruvate was due to reversible pyruvate:ferredoxin oxidoreductase (PFOR), which can
166 form pyruvate by combining unlabeled CO₂ and acetyl group derived from the reductive acetyl-CoA
167 pathway. With phosphoenolpyruvate (PEP) remaining mostly labeled, the contrasting pyruvate
168 labeling indicated that pyruvate kinase (PEP + ADP → Pyr + ATP) was forward-driven to produce
169 ATP.

170 Interestingly, serine, glycine, as well as other amino acids derived from pyruvate and TCA cycle
171 intermediates were also half-labeled (**Fig. 4C, Supplementary Table 3**). These labeling data
172 suggested shared usage of central metabolism, where glucose and CO₂ jointly contributed to the
173 TCA cycle (and thus non-aromatic amino acid biosynthesis). However, because glycolysis and the
174 pentose phosphate pathway (and thus the synthesis of nucleotide ribose rings and aromatic amino
175 acids) were driven mainly by glucose, cells incorporated more carbons from glucose. Therefore,
176 despite the simultaneous consumption of CO₂ and glucose, lack of observable net CO₂ fixation was
177 the result of cells prioritizing ATP production (and cell growth). Prioritizing ATP production
178 involves faster glycolysis via faster glucose uptake. This substrate hierarchy favoring glucose
179 subsequently led to excessive pyruvate decarboxylation via PFOR (**Fig. 4D, Supplementary Table**
180 **4**) which, together with CO₂-producing biosynthetic pathways (**Supplementary Fig. 6**), outpaced
181 CO₂ incorporation.

182 **Accelerating acetate production from CO₂ by decoupling e⁻ supply from decarboxylation**

183 Since undesirable decarboxylation is coupled to the PFOR step for e⁻ generation from glucose, we
184 aimed to limit the function of glucose as an e⁻ source and to stimulate net CO₂ incorporation. On the
185 other hand, sufficient ATP is still required from glucose through pyruvate kinase to avoid slow
186 metabolism and sustain CO₂ reduction. We note that acetate production via the reductive acetyl-
187 CoA pathway does not consume ATP leading to cell maintenance (e.g., housekeeping) being the only
188 ATP requirement for converting CO₂ to acetate (**Supplementary Fig. 7**). Hence, we implemented
189 glucose-limiting culture environments in a chemostat to reduce the rate of glycolysis such that it
190 supplies the required ATP but overall decarboxylation is slowed (**Fig. 5A**). To compensate for the
191 decreased e⁻ availability, cells were provided with H₂ as a carbon-free e⁻ source that yields reducing
192 agents without CO₂ generation. In addition, low dilution rates (0.009 and 0.017 hr⁻¹) were selected
193 to minimize biomass formation and maximize cell residence time in the reactor.

194 Using this glucose doping system, productivities and yields at various fractions of electrons derived
195 from glucose versus H₂ were obtained (**Fig. 5B**). In this plot, we also included batch results with or
196 without H₂ in the headspace (**Supplementary Table 5**). Interestingly, the presence of H₂ decreased
197 glucose consumption rate, shifting carbon substrate preferences towards CO₂ (**Supplementary Fig.**
198 **8**). At steady state, acetate concentration in the effluent from the chemostat could exceed 13 g/L.
199 With decreasing fractions of electrons from glucose, acetate production rate could be more than 80
200 times as fast as the glucose feed rate, and the carbon yield monotonically increased to >80 g acetate
201 produced per g glucose consumed. This high yield indicated that the overwhelming majority of
202 acetate and biomass was derived from CO₂ rather than glucose. While cell growth rates were slow
203 in the chemostat (growth rate = dilution rate), acetate production remained fast (**Fig. 5B**).
204 Importantly, we found that, at 2% of e⁻ from glucose, glucose doping simultaneously enabled a very
205 high yield (>50 g acetate/g glucose) and a substantial acetate productivity (>9 mmol gCDW⁻¹ hr⁻¹,
206 ~1/3 of the maximum observed productivity).

207 Across the glucose+H₂ energy landscape, CO₂ fixation rates peaked at 52.7 mmol gCDW⁻¹ hr⁻¹ (2.3 g
208 gCDW⁻¹ hr⁻¹) (**Fig. 5C**). Such high rates implied that we not only decreased CO₂ generation from
209 pyruvate decarboxylation but also increased the reductive acetyl-CoA pathway flux. Furthermore,
210 the maximum rate occurring between the two extremes (glucose-only and H₂-only) demonstrated
211 that CO₂ fixation rate is determined by a balance between reducing agents and ATP supplied via H₂
212 and glucose, respectively. Thus, by controlled glucose doping, we decoupled e⁻ supply from
213 decarboxylation, shifted cellular metabolism towards favoring CO₂ utilization over glucose, and
214 achieved rapid and continuous CO₂ conversion into acetate.

215 **Coordination of “doped” acetogenesis and lipogenesis**

216 Coordinating acetogenesis and lipogenesis allows CO₂-to-acetate-to-lipid conversion. Interestingly,
217 the observed acetate and fatty acid productivities from glucose- and gluconate-doping (V₁₂)
218 exceeded not only the measured productivities with individual substrates (V₁ or V₂) but also the
219 expected productivity for the two substrates combined (V₁ + V₂) (**Fig. 6A**). The expected
220 productivity was linearly extrapolated from the combination of supplemental glucose feeding with
221 CO₂+H₂ batch fermentation for acetogenesis and the combination of supplemental gluconate
222 feeding with acetate batch fermentation for lipogenesis (**Supplementary Information**).

223 We attributed the observed synergy (V₁₂>V₁+V₂) to complementary substrate cofeeding. While our
224 ¹³C labeling experiments showed the roles of glucose and gluconate in ATP and cofactor synthesis,
225 respectively, we sought to define the theoretical framework that illustrates the feasibility of this
226 synergy. To this end, stoichiometric analysis of the different fates of individual substrates was
227 combined with experimentally measured rates of single-substrate acetogenesis and lipogenesis.
228 The maximum carbon, ATP, and electron attainable with mixed substrates were then evaluated for
229 the two processes (**Supplementary Information**). We identified that the ATP and NADPH
230 generation by glucose and gluconate doping relieved the limiting ingredients for acetate and lipid
231 synthesis, respectively, and, in conjunction with the primary substrates, better balanced the energy
232 and cofactor ratio requirements for reduced bioproduct synthesis (**Fig. 6B**).

233 In terms of organic carbon yield, the integrated acetogenesis-lipogenesis process converted 1 g of
234 glucose to ~13 g of lipids (0.154 g lipids/g acetate × ~82 g acetate/g glucose) by extensive CO₂

235 utilization. Increasing mass transfer rates of gases improves H₂ (and CO₂) utilization efficiency, and
236 it has been reported that ~95% of supplied H₂ can be used by commercial CO₂-fixing microbes^{30,31}.
237 By continuously converting CO₂ and H₂ to lipids via coordinated acetogenesis and lipogenesis, 38%
238 of energy from H₂ was stored as lipids and 14% as yeast biomass (**Fig. 6C**). Nearly all carbons
239 (~99%) in lipids originated from CO₂.

240 To further explore the potential of our synergistic cofeeding approach, we applied the
241 stoichiometric analysis to other acetyl-CoA derived products and determined the gains in
242 productivities (**Fig. 6D and Supplementary Information**). Similar to the results for fatty acids, the
243 model predicted synergy between the substrate pair in producing other reduced compounds such
244 as polyhydroxybutyrate (PHB) and isopentenyl pyrophosphate (IPP, precursor for isoprenoids),
245 leading to increases in productivities over the extrapolated sum ($V_{12} > V_1 + V_2$). Therefore, our
246 substrate cofeeding strategy may stimulate conversion of CO₂ into a wide array of advanced
247 bioproducts.

248 **Discussion**

249 One of the greatest biotechnological challenges is engineering metabolism. Current engineering
250 efforts often focus on funneling metabolic fluxes through product synthesis pathways via
251 assembling various gene pools and knocking out competing pathways with existing genetic tools³².
252 In addition, most processes start from sugars as the sole substrate, which inherently causes some
253 metabolic intermediates to be out of balance and surplus components to be wasted because of the
254 differences in chemical properties between the substrate and the product. This further necessitates
255 the use of genetic engineering for flux rewiring in order to achieve industrially relevant production
256 metrics. Such approaches set a limit on the choice of microbial hosts based on genetic
257 manipulability and the existing strategies are not generalizable to all organisms.

258 Here we presented the potential of mixed substrate cofeeding as a generalizable method and a
259 more effective starting point for bioproduct synthesis. As the first step, we overcame the difficulties
260 that arise due to organisms' preferential substrate usage. Controlled continuous feeding of a
261 preferred substrate as a metabolic dopant did not inhibit the consumption of the less favored
262 substrate. Using this approach, we enhanced the utilization of CO₂ and acetate, which are typically
263 the end products of metabolism and therefore least preferred by organisms. This was demonstrated
264 in both *M. thermacetica* and *Y. lipolytica*, two organisms with distinct metabolism and genetic
265 manipulability, using various substrates (glucose and H₂/CO₂ as well as acetate and gluconate).
266 Correspondingly, we expect this design to be widely applicable to other substrates and organisms.

267 Surprisingly, substrate cofeeding synergistically enhanced product synthesis. In both cases, the
268 total product carbon flux resulting from co-utilized substrates (V_{12}) exceeded the sum of the
269 individual substrate fluxes ($V_1 + V_2$). However, previous models describing substrate co-utilization
270 have overlooked this synergistic effect¹¹. The observation of $V_{12} > V_1 + V_2$ could be explained by the
271 two substrates having distinct yet complementary functions in cellular metabolism. Our
272 stoichiometric analysis of metabolic requirements and burdens suggested that glucose and
273 gluconate as dopant substrates could indeed complement ATP and NADPH generation, alleviating
274 the limitations seen in acetogenesis and lipogenesis, respectively. Importantly, the observed

275 significant enhancements in CO₂ and acetate reduction metabolism required only minor addition of
276 “valuable” glucose and gluconate.

277 To understand how the dopant substrates can strikingly achieve such efficiency in enhancing
278 reductive metabolism, we also elucidated the underlying mechanisms. Tracing ¹³C-labeled glucose
279 and gluconate revealed that nearly all of these supplements went into ATP and NADPH production,
280 respectively. We identified pyruvate kinase (PEP+ADP → Pyr+ATP) in *M. thermoacetica* and the
281 pentose cycle (6PG → R5P → F6P → G6P → 6PG + 2 NADPH) in *Y. lipolytica* to be important cofactor
282 generating steps. In particular, activating pyruvate kinase by cofeeding glucose solved the challenge
283 of slow CO₂ fixation, which is due to ATP-limited metabolism in autotrophic fermentations^{31,33}.
284 Activating the pentose cycle by cofeeding gluconate solved the challenge of limited NADPH
285 production through oxPPP in acetate-fed cells. Therefore, we rewired metabolism without genetic
286 engineering by cofeeding dopant substrates.

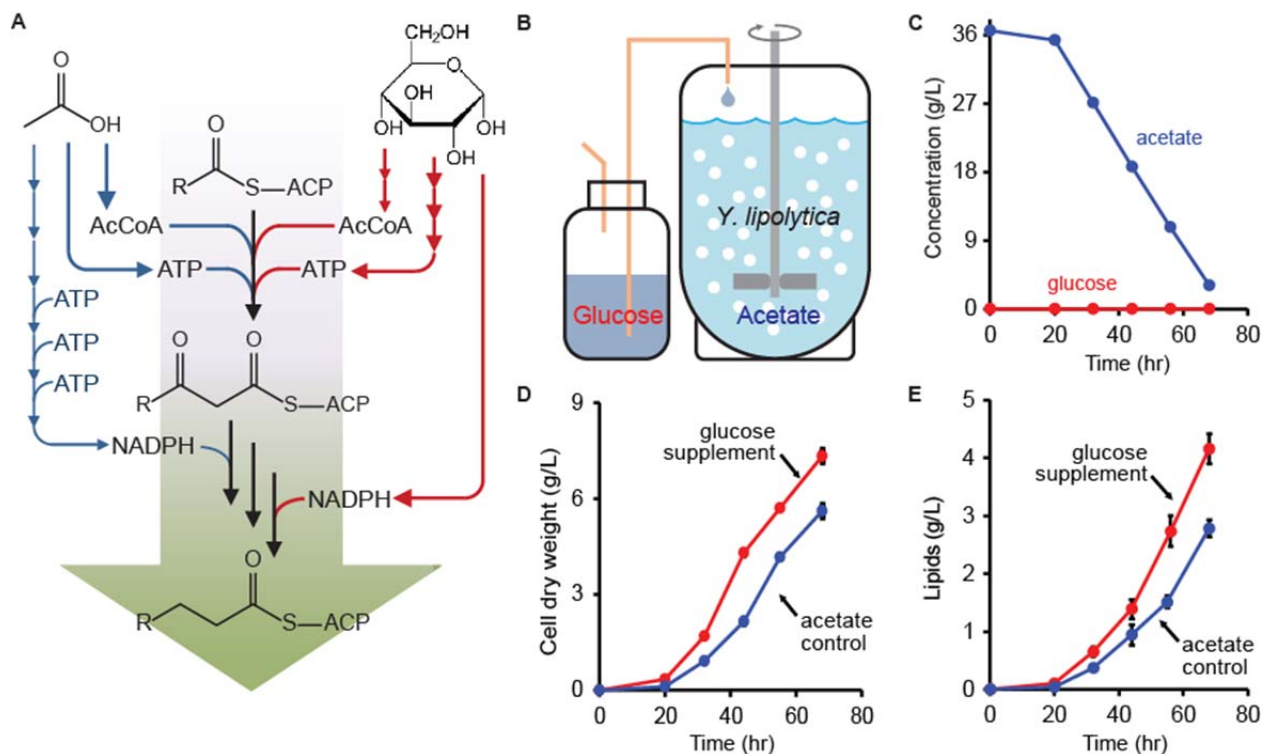
287 Finally, akin to the widespread use of dopants in the electronics industry to enhance material
288 properties, we envision the dopant substrate cofeeding scheme becoming valuable in a wide array
289 of biotechnological applications. Our demonstration of CO₂/H₂-to-acetate-to-lipids conversion at
290 high productivity and energetic efficiency serves as an exemplary renewable energy storage
291 strategy using substrates that do not interfere with food supply. Since acetate is closely related to
292 acetyl-CoA, a focal point in many metabolic pathways, other acetate-based processes applying
293 proper doping substrates could enable rapid synthesis of a wide repertoire of bioproducts such as
294 fatty acid derived oleochemicals³⁴ and mevalonate pathway derived natural products³⁵. By coupling
295 this to the glucose-doped acetogenesis, CO₂ could become the initial feedstock for all subsequent
296 acetate-driven processes, benefiting both the environment and carbon economy. Moreover, the
297 metabolic enhancements by cofeeding superior substrates is not limited to CO₂- and acetate-based
298 fermentations. The imbalance of carbon building blocks, cofactors, and energy with respect to the
299 desired product requirement can also be seen in many other single-substrate substrate
300 bioconversions. In these cases, identification of complementary substrates and implementation of
301 controlled dopant substrate cofeeding would optimally coordinate pathway usage for superior
302 biosynthesis. Consequently, substrates previously considered infeasible for industrial bioprocesses
303 due to limited productivity may become well-suited as economically and technologically viable
304 feedstocks³⁶.

305 **Acknowledgments** The authors would like to thank Drs. Caroline Lewis and Elizaveta Freinkman
306 for their help with LC-MS. This research was supported by U.S. Department of Energy grants DE-
307 AR0000433, DE-SC0008744 and DE-SC0012377 as well as Mobility Plus Fellowship
308 1284/MOB/IV/2015/0.

309 **Author Contributions** J.O.P, N.L., and G.S. designed the study and wrote the paper. J.O.P., N.L. and
310 K.M.H performed experiments and flux analysis. J.O.P., N.L., B.M.W., and C.V. developed LC-MS and
311 GC-MS methods. J.O.P., N.L., D.F.E., J.X. designed the bioreactors. J.O.P. and M.A.I. developed the
312 updated metabolic model. J.O.P., N.L., K.Q., Z.L., P.R.G. and G.S. analyzed the data.

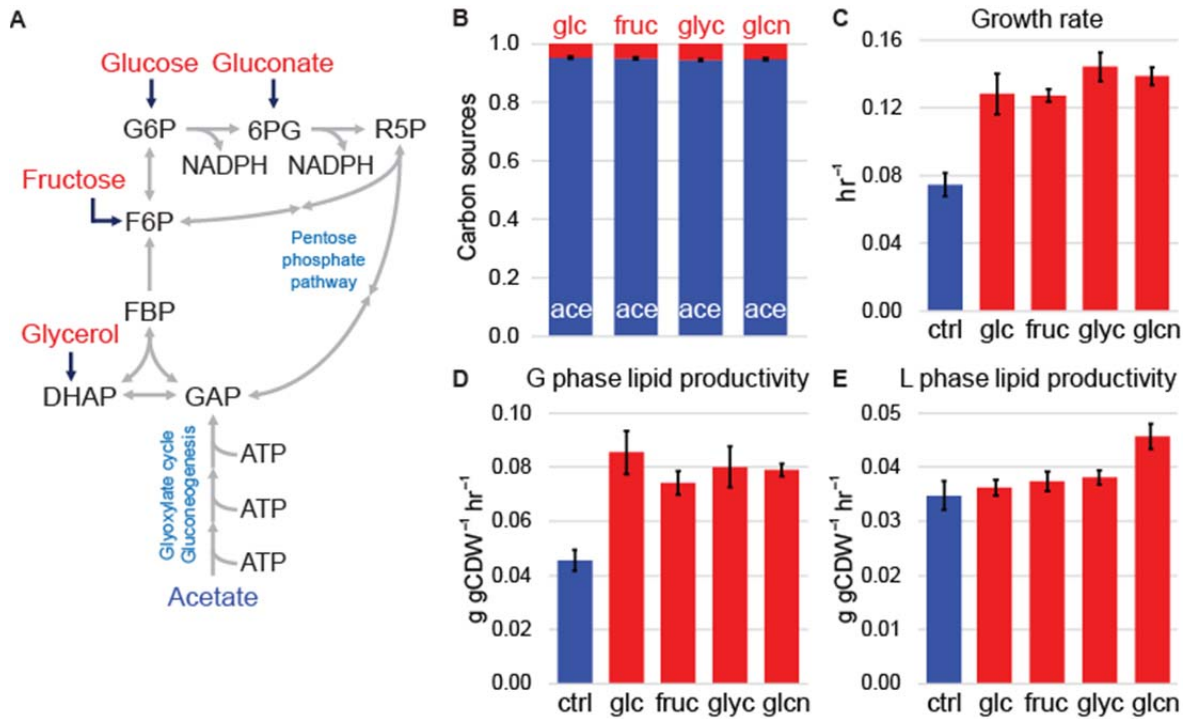
313

314 **Figures**



315

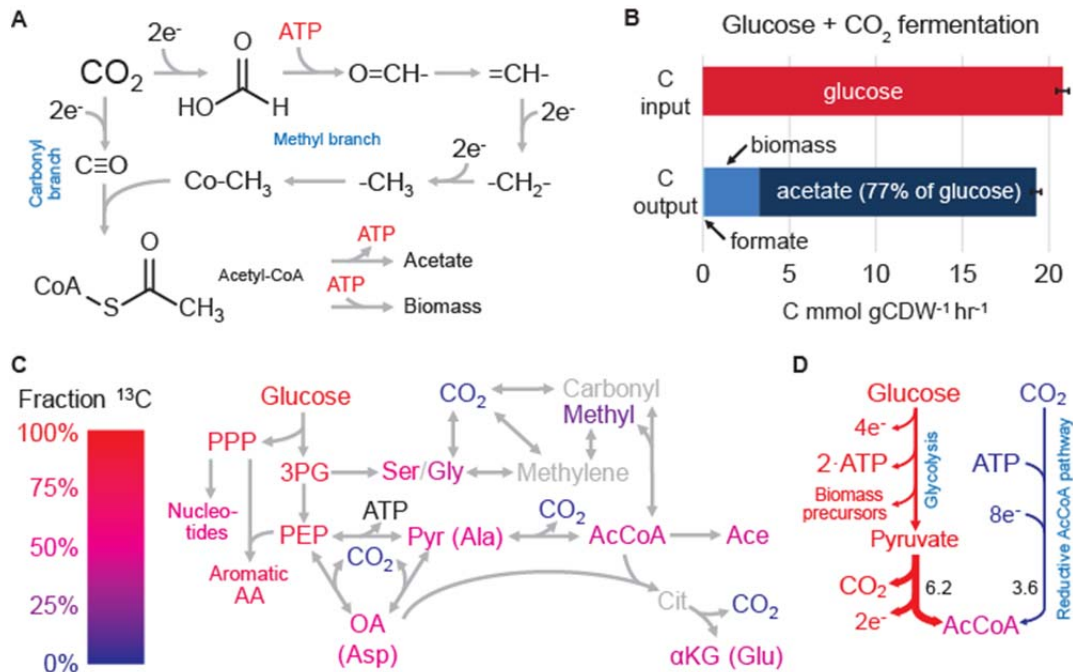
316 **Figure 1. Continuous glucose cofeeding relieves repression of acetate in *Y. lipolytica*.** (A)
 317 Acetate can efficiently support acetyl-CoA and ATP generation through the TCA cycle but not
 318 NADPH generation, which requires many enzymatic steps and ATP. Glucose, on the other hand, can
 319 produce NADPH more directly through oxPPP. (B) Since glucose batch feeding suppresses acetate
 320 consumption, glucose was continuously supplemented in small quantities to the acetate culture. (C)
 321 Despite the continuous feeding of glucose, its concentration in the reactor remained at 0 and
 322 acetate concentration decreased. Thus, the fed-batch system enabled simultaneous consumption of
 323 acetate and glucose. (D) Biomass and (E) lipid production was faster and higher with glucose-
 324 “doping” compared to the acetate-only control.



325

326 **Figure 2. Cofeeding substrates near oxidative pentose phosphate pathway accelerates cell**
 327 **growth and lipogenesis from acetate. (A)** Glucose, fructose, glycerol, and gluconate enter central
 328 carbon metabolism through upper glycolysis and PPP. **(B)** Supplementation of these four substrates
 329 accounted for ~5% of the total carbon consumed by the cells and the primary carbon source was
 330 acetate. **(C)** Specific growth rates nearly doubled with substrate cofeeding compared to the acetate-
 331 only control. **(D)** Growth phase (nitrogen-replete) specific lipid productivity nearly doubled with
 332 substrate cofeeding. **(E)** Lipogenic phase (nitrogen-depleted) specific lipid productivity was mildly
 333 enhanced by glucose, fructose, or glycerol supplementation. Gluconate-“doping” significantly
 334 outperformed the other conditions.

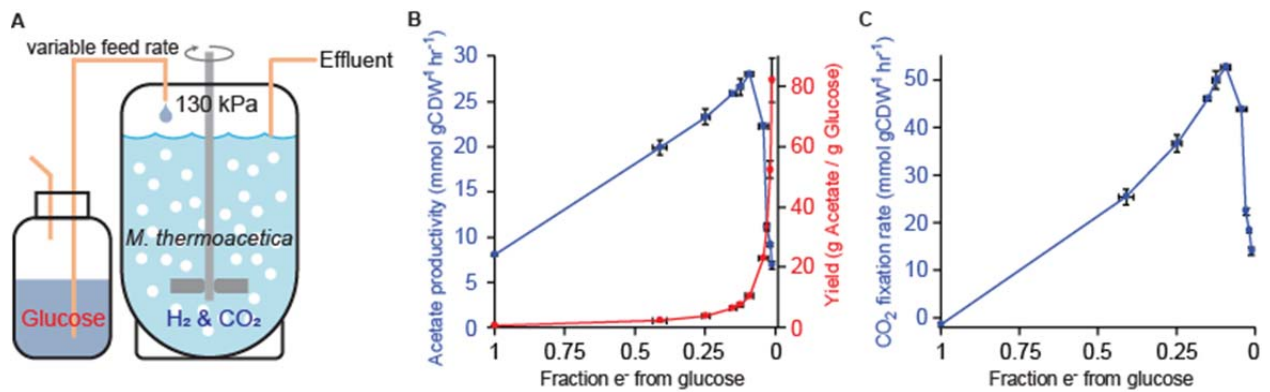
335



345

346 **Figure 4. Glucose generates ATP for CO_2 fixation but leads to decarboxylation in *M.***
 347 ***thermoacetica*.** (A) The reductive acetyl-CoA pathway consists of the carbonyl and methyl
 348 branches for conversion of CO_2 into acetyl group. The methyl branch requires ATP. (B) Analysis of
 349 carbon input and output in batch cofeeding of *M. thermoacetica* with glucose and CO_2 revealed the
 350 preferential use of glucose. (C) Batch cofeeding [$\text{U-}^{13}\text{C}_6$]glucose and CO_2 revealed the simultaneous
 351 use of glucose and CO_2 . Glucose carbons contributed mainly to glycolysis and PPP while partially to
 352 TCA cycle. A substantial fraction of TCA carbons was traced to CO_2 . (D) Despite simultaneous
 353 utilization of CO_2 , preferred glucose use led to undesirable decarboxylation outpacing CO_2 uptake.
 354 Flux values are in $\text{mmol gCDW}^{-1} \text{hr}^{-1}$ of acetyl-CoA.

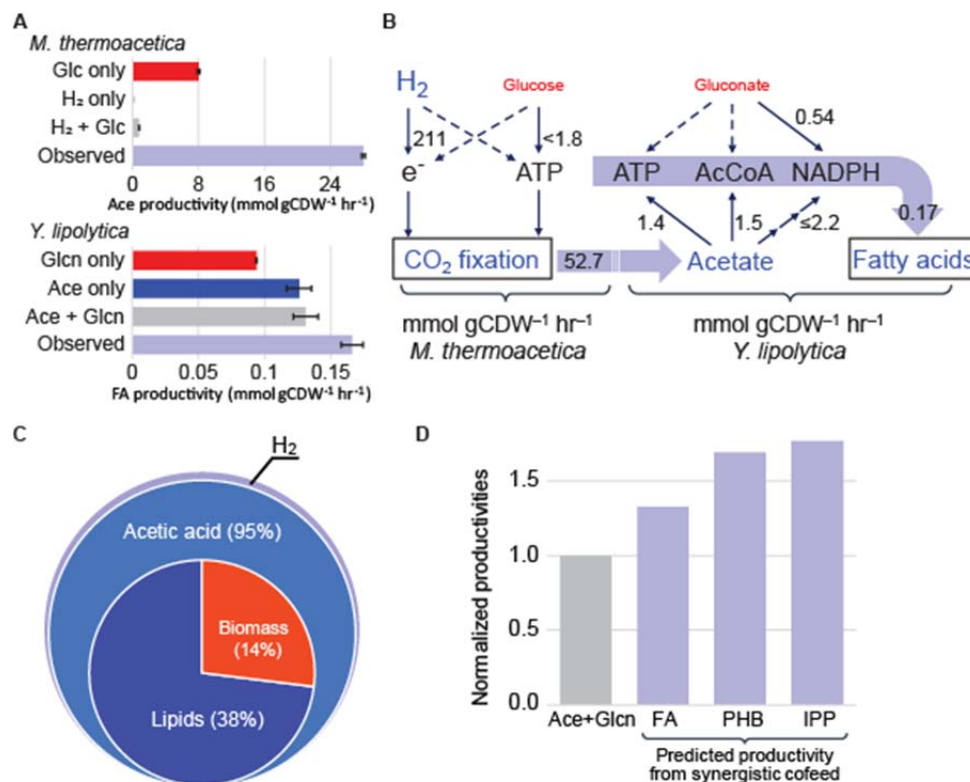
355



356

357 **Figure 5. Continuous glucose cofeeding accelerates acetogenesis from CO₂ fixation at the**
 358 **autotrophic limit. (A)** Since glucose batch feeding leads to undesirable decarboxylation, glucose
 359 was continuously supplemented in small quantities to gas-fermenting *M. thermoacetica* culture.
 360 **(B,C)** Acetate productivity, yield, and CO₂ fixation rate at varying ratios of electrons (e⁻) derived
 361 from H₂ and glucose. The plots include both batch and chemostat data (**Supplementary Table 5**).
 362 **(B)** Acetate productivity peaked when 91% of e⁻ were derived from H₂ and 9% glucose. On the
 363 other hand, carbon yield (acetate produced per glucose consumed) increased with increasing
 364 fraction of electrons from H₂. **(C)** CO₂ fixation rate peaked when 9% of e⁻ were derived from glucose
 365 and remained high near the autotrophic limit.

366



367

368 **Figure 6. Synergy and coordination of substrate cofeeding accelerate the conversion of CO₂**
 369 **and H₂ into lipids. (A)** Glucose- and gluconate-doping resulted in synergy that accelerated
 370 acetogenesis and lipogenesis beyond the linear extrapolation of additional carbon supplement. **(B)**
 371 The maximum CO₂ fixation and fatty acid production rates were attained by cofeeding glucose and
 372 gluconate in limiting quantities. Stoichiometric analysis of metabolic requirements and burdens
 373 revealed the key role of glucose and gluconate in generating ATP and NADPH. The dashed arrows
 374 denote negligible contributions. **(C)** In terms of energy efficiency, 95% of H₂ energy can be stored as
 375 acetate by *M. thermoacetica* and 55% of acetate energy can be stored as lipids by *Y. lipolytica*.
 376 Coordination of acetogenesis and lipogenesis enabled storage of 38% of H₂ energy as lipids and
 377 14% as biomass. **(D)** The cofeeding approach can also be applied to synthesizing other products
 378 with predicted synergistic productivity that exceeds the sum of individual-substrate productivities.

379

380 **References**

- 381 1 Ledesma-Amaro, R. & Nicaud, J. M. Metabolic Engineering for Expanding the Substrate
382 Range of *Yarrowia lipolytica*. *Trends Biotechnol* **34**, 798-809,
383 doi:10.1016/j.tibtech.2016.04.010 (2016).
- 384 2 Atsumi, S., Hanai, T. & Liao, J. C. Non-fermentative pathways for synthesis of branched-
385 chain higher alcohols as biofuels. *Nature* **451**, 86, doi:10.1038/nature06450 (2008).
- 386 3 Xue, Z. *et al.* Production of omega-3 eicosapentaenoic acid by metabolic engineering of
387 *Yarrowia lipolytica*. *Nat Biotechnol* **31**, 734-740, doi:10.1038/nbt.2622 (2013).
- 388 4 Qiao, K. J., Wasylenko, T. M., Zhou, K., Xu, P. & Stephanopoulos, G. Lipid production
389 in *Yarrowia lipolytica* is maximized by engineering cytosolic redox metabolism. *Nature*
390 *biotechnology* **35**, 173-177, doi:10.1038/nbt.3763 (2017).
- 391 5 Kita, A. *et al.* Development of genetic transformation and heterologous expression
392 system in carboxydrotrophic thermophilic acetogen *Moorella thermoacetica*. *J Biosci*
393 *Bioeng* **115**, 347-352, doi:10.1016/j.jbiosc.2012.10.013 (2013).
- 394 6 Monod, J. Recherches sur la croissance des cultures bacteriennes. (1942).
- 395 7 Aristilde, L., Lewis, I. A., Park, J. O. & Rabinowitz, J. D. Hierarchy in Pentose Sugar
396 Metabolism in *Clostridium Acetobutylicum*. *Appl Environ Microbiol*,
397 doi:10.1128/AEM.03199-14 (2014).
- 398 8 Goerke, B. & Stulke, J. Carbon catabolite repression in bacteria: many ways to make the
399 most out of nutrients. *Nat Rev Microbiol* **6**, 613-624, doi:Doi 10.1038/Nrmicro1932
400 (2008).
- 401 9 Bren, A. *et al.* Glucose becomes one of the worst carbon sources for *E.coli* on poor
402 nitrogen sources due to suboptimal levels of cAMP. *Sci Rep* **6**, 24834,
403 doi:10.1038/srep24834 (2016).
- 404 10 Joshua, C. J., Dahl, R., Benke, P. I. & Keasling, J. D. Absence of diauxie during
405 simultaneous utilization of glucose and Xylose by *Sulfolobus acidocaldarius*. *J Bacteriol*
406 **193**, 1293-1301, doi:10.1128/JB.01219-10 (2011).
- 407 11 Hermsen, R., Okano, H., You, C., Werner, N. & Hwa, T. A growth-rate composition
408 formula for the growth of *E.coli* on co-utilized carbon substrates. *Mol Syst Biol* **11**, 801,
409 doi:10.15252/msb.20145537 (2015).
- 410 12 Kanno, M., Carroll, A. L. & Atsumi, S. Global metabolic rewiring for improved CO₂
411 fixation and chemical production in cyanobacteria. *Nature communications* **8**,
412 doi:10.1038/Ncomms14724 (2017).
- 413 13 Martinez, K. *et al.* Couitilization of glucose and glycerol enhances the production of
414 aromatic compounds in an *Escherichia coli* strain lacking the phosphoenolpyruvate:
415 carbohydrate phosphotransferase system. *Microb Cell Fact* **7**, 1, doi:10.1186/1475-2859-
416 7-1 (2008).
- 417 14 Meyer, F. *et al.* Methanol-essential growth of *Escherichia coli*. *Nature communications* **9**,
418 doi:10.1038/S41467-018-03937-Y (2018).
- 419 15 Garcia Sanchez, R. *et al.* Improved xylose and arabinose utilization by an industrial
420 recombinant *Saccharomyces cerevisiae* strain using evolutionary engineering. *Biotechnol*
421 *Biofuels* **3**, 13, doi:10.1186/1754-6834-3-13 (2010).
- 422 16 Kim, S. M. *et al.* Simultaneous utilization of glucose and xylose via novel mechanisms in
423 engineered *Escherichia coli*. *Metab Eng* **30**, 141-148, doi:10.1016/j.ymben.2015.05.002
424 (2015).

- 425 17 Jones, S. W. *et al.* CO₂ fixation by anaerobic non-photosynthetic mixotrophy for
426 improved carbon conversion. *Nat Commun* **7**, 12800, doi:10.1038/ncomms12800 (2016).
- 427 18 Bowes, G., Hageman, R. H. & Ogren, W. L. Light Saturation, Photosynthesis Rate, RuDP
428 Carboxylase Activity, and Specific Leaf Weight in Soybeans Grown under Different
429 Light Intensities. *Crop Sci* **12**, 77-& (1972).
- 430 19 Xu, J., Liu, N., Qiao, K., Vogg, S. & Stephanopoulos, G. Application of metabolic
431 controls for the maximization of lipid production in semicontinuous fermentation. *Proc*
432 *Natl Acad Sci U S A* **114**, E5308-E5316, doi:10.1073/pnas.1703321114 (2017).
- 433 20 Ratledge, C. & Wynn, J. P. The biochemistry and molecular biology of lipid
434 accumulation in oleaginous microorganisms. *Advances in applied microbiology* **51**, 1-51
435 (2002).
- 436 21 Qiao, K. *et al.* Engineering lipid overproduction in the oleaginous yeast *Yarrowia*
437 *lipolytica*. *Metab Eng* **29**, 56-65, doi:10.1016/j.ymben.2015.02.005 (2015).
- 438 22 Fontanille, P., Kumar, V., Christophe, G., Nouaille, R. & Larroche, C. Bioconversion of
439 volatile fatty acids into lipids by the oleaginous yeast *Yarrowia lipolytica*. *Bioresource*
440 *Technology* **114**, 443-449, doi:https://doi.org/10.1016/j.biortech.2012.02.091 (2012).
- 441 23 Liu, N., Qiao, K. & Stephanopoulos, G. (13)C Metabolic Flux Analysis of acetate
442 conversion to lipids by *Yarrowia lipolytica*. *Metab Eng* **38**, 86-97,
443 doi:10.1016/j.ymben.2016.06.006 (2016).
- 444 24 Gancedo, J. M. Carbon catabolite repression in yeast. *Eur J Biochem* **206**, 297-313
445 (1992).
- 446 25 Casazza, J. P. & Veech, R. L. The Interdependence of Glycolytic and Pentose Cycle
447 Intermediates in Ad-Libitum Fed Rats. *J Biol Chem* **261**, 690-698 (1986).
- 448 26 Ragsdale, S. W. & Pierce, E. Acetogenesis and the Wood-Ljungdahl pathway of CO₂(₂)
449 fixation. *Biochimica et biophysica acta* **1784**, 1873-1898,
450 doi:10.1016/j.bbapap.2008.08.012 (2008).
- 451 27 Mall, A. *et al.* Reversibility of citrate synthase allows autotrophic growth of a
452 thermophilic bacterium. *Science* **359**, 563-567, doi:10.1126/science.aao2410 (2018).
- 453 28 Nunoura, T. *et al.* A primordial and reversible TCA cycle in a facultatively
454 chemolithoautotrophic thermophile. *Science* **359**, 559-563, doi:10.1126/science.aao3407
455 (2018).
- 456 29 Schuchmann, K. & Muller, V. Autotrophy at the thermodynamic limit of life: a model for
457 energy conservation in acetogenic bacteria. *Nat Rev Microbiol* **12**, 809-821,
458 doi:10.1038/nrmicro3365 (2014).
- 459 30 Daniell, J., Köpke, M. & Simpson, S. Commercial Biomass Syngas Fermentation.
460 *Energies* **5**, 5372 (2012).
- 461 31 Hu, P., Rismani-Yazdi, H. & Stephanopoulos, G. Anaerobic CO₂ fixation by the
462 acetogenic bacterium *Moorella thermoacetica*. *AIChE Journal* **59**, 3176-3183,
463 doi:10.1002/aic.14127 (2013).
- 464 32 Blazeck, J. *et al.* Harnessing *Yarrowia lipolytica* lipogenesis to create a platform for lipid
465 and biofuel production. *Nat Commun* **5**, 3131, doi:10.1038/ncomms4131 (2014).
- 466 33 Daniel, S. L., Hsu, T., Dean, S. I. & Drake, H. L. Characterization of the H₂- and CO-
467 dependent chemolithotrophic potentials of the acetogens *Clostridium thermoaceticum* and
468 *Acetogenium kivui*. *J Bacteriol* **172**, 4464-4471 (1990).

- 469 34 Ledesma-Amaro, R., Dulermo, R., Niehus, X. & Nicaud, J. M. Combining metabolic
470 engineering and process optimization to improve production and secretion of fatty acids.
471 *Metab Eng* **38**, 38-46, doi:10.1016/j.ymben.2016.06.004 (2016).
472 35 Martin, V. J. J., Pitera, D. J., Withers, S. T., Newman, J. D. & Keasling, J. D.
473 Engineering a mevalonate pathway in *Escherichia coli* for production of terpenoids.
474 *Nature biotechnology* **21**, 796-802, doi:10.1038/nbt833 (2003).
475 36 Haynes, C. A. & Gonzalez, R. Rethinking biological activation of methane and
476 conversion to liquid fuels. *Nat Chem Biol* **10**, 331-339, doi:10.1038/nchembio.1509
477 (2014).
478

479

480

481 **Methods**

482 **Strains and culture conditions**

483 *Yarrowia lipolytica* strains based on the ACCDGA strain (MTYL065)³⁷ were pre-cultured at 30 °C in
484 14 mL test tubes containing YPD media (20 g/L glucose, 20 g/L peptone, 10 g/L yeast extract). After
485 24 hr, 1 mL culture was transferred to a shake flask containing 40 mL of acetate media (50 g/L
486 sodium acetate, 1.7 g/L YNB-AA-AS, and 1.34 g/L ammonium sulfate). The shake flask culture was
487 carried out for 24 hr to adapt the cells to acetate. Afterwards, the cells were pelleted at 18,000 g for
488 5 min, washed once with acetate media, and used for inoculation at an initial OD₆₀₀ of 0.05 for all *Y.*
489 *lipolytica* experiments.

490 Mixed substrate batch cultures were carried out in shake flasks with 40 mL of acetate media except
491 that 6 mol% of the total carbon from acetate was replaced with the supplemental substrate
492 (glucose, fructose, glycerol, or gluconate). Continuous fed-batch supplementation cultures were
493 carried out in 250 mL bioreactors (Applikon Biotechnology) with 150 mL working volume. Acetate
494 media was used under batch conditions while the supplemented substrate was continuously fed at
495 a rate of 0.13 mmol C/hr. For the acetate-only control case, the supplemented substrate was
496 replaced with acetate and fed at the same rate to ensure that cells had equal amounts of carbon
497 substrates throughout all conditions. All bioreactor cultures were carried out at 30 °C, pH 7.0
498 (controlled with 10 wt% sulfuric acid), and 0.2 LPM air sparging. The dissolved oxygen levels were
499 controlled at 20% during the growth phase and ~2% during the lipogenic phase for optimal lipid
500 production and minimal citrate excretion⁴. For gluconate ¹³C tracing experiments, natural gluconate
501 in the supplementation feed stream was replaced with [U-¹³C₆]gluconate (99%, Cambridge Isotope
502 Laboratories).

503 In all *Y. lipolytica* experiments having gluconate as a substrate, an ACCDGA strain overexpressing its
504 native gluconate kinase (glucK) under the *TEF_{in}* promoter was used. The expression of *TEF_{in}*-glucK
505 was performed through genome integration. This was to ensure that gluconate uptake and
506 incorporation into central carbon metabolism was not inhibited by inadequate levels of the kinase.
507 All other experiments were performed using the same ACCDGA strain with an empty control vector

508 integrated into the genome. Overexpressing gluconate kinase did not have any appreciable effects
509 on the strain's capability to produce lipids on acetate, as shown in **Supplementary Fig. 9**.

510 *Moorella thermoacetica* (ATCC 39073 and 49707) were cultured in balch-type tubes containing
511 culture medium with 8 g/L glucose, 7.5 g/L NaHCO₃, 7 g/L KH₂PO₄, 5.5 g/L K₂HPO₄, 2 g/L
512 (NH₄)₂SO₄, 0.5 g/L MgSO₄ • 7H₂O, 0.3 g/L cysteine, 0.02 g/L CaCl₂ • 2H₂O, 1% (v/v) trace minerals
513 (ATCC MD-TMS), and 1% (v/v) vitamins (ATCC MD-VS) at 55 °C pH 6.8. Cysteine scavenged
514 residual dissolved oxygen in the medium³⁸. The headspace was pressurized to either 170 kPa with
515 CO₂ or 240 kPa with 80:20 H₂/CO₂. For ¹³C tracing experiments, natural glucose was replaced with
516 [U-¹³C₆]glucose (99%, Cambridge Isotope Laboratories) and the headspace was pressurized to 170
517 kPa with natural CO₂. The balch-tube cultures were incubated inside a strictly anoxic glovebox with
518 magnetic stirring.

519 For bioreactor experiments, *M. thermoacetica* (ATCC 49707) was cultured in a strictly anoxic vessel
520 with pH and temperature control set to 6.6 (using 10M sodium hydroxide) and 55°C. Low glucose
521 but otherwise identical culture media were fed as follows (media glucose concentrations and media
522 feed rates): 0.25 g/L at 11.5 mL/hr; 0.25 g/L at 9.1 mL/hr; 0.25 g/L at 6.9 mL/hr; 0.25 g/L at 4.3
523 mL/hr; 0.25 g/L at 2.3 mL/hr; 0.25 g/L at 1.2 mL/hr; and 0.13 g/L at 1.2 mL/hr. The rate of
524 effluent was the same to keep the culture volume constant at 135 mL. H₂ and CO₂ were mixed at
525 60:40 and sparged into the culture at 200 mL/min. The headspace pressure was maintained at 130
526 kPa. All the data and conditions are shown in **Supplementary Table 5**.

527 **Metabolite extraction and measurement**

528 To extract metabolites, *Y. lipolytica* cells were collected during exponential and lipogenic phases.
529 Cells were filtered on 0.45 µm nylon membrane filters and immediately transferred to a precooled
530 40:40:20 acetonitrile/methanol/water solution. After 20 minutes at -20°C, the filters were washed,
531 and extracts were moved to Eppendorf tubes. The samples were then centrifuged for five minutes
532 and the supernatants were dried under nitrogen.

533 In mid-exponential phase, the *M. thermoacetica* cultures were collected from balch-type tubes using
534 syringes inside the anaerobic glovebox. Immediately after, cellular metabolism was quenched and
535 metabolites were extracted by quickly transferring filtered cells (on 0.2 µm nylon membrane filter)
536 to plates containing precooled 80% acetonitrile on ice³⁹. After 20 minutes at 4°C, the membrane
537 filters were washed, and the metabolite extracts were moved to Eppendorf tubes. The supernatants
538 were obtained after five minutes of centrifugation and lyophilized.

539 Dried samples were resuspended in HPLC-grade water for LC-MS analysis. These samples were
540 analyzed on a Dionex UltiMate 3000 UPLC system (Thermo) with a ZIC-pHILIC (5 µm polymer
541 particle) 150 × 2.1 mm column (EMD Millipore) coupled to a QExactive orbitrap mass spectrometer
542 (Thermo) by electrospray ionization. With 20 mM ammonium carbonate, 0.1% ammonium
543 hydroxide as solvent A and acetonitrile as solvent B, the chromatographic gradient was run at a
544 flow rate of 0.150 mL/min as a linear gradient from 80% B to 20% B between 0 and 20 mins, a
545 linear gradient from 20% B to 80% B between 20 and 20.5 mins, and 80% B held from 20.5 to 28
546 mins. The column and autosampler tray temperature were at 25 °C and 4 °C. The mass
547 spectrometer was operated in polarity switching mode scanning a range of 70-1,000 m/z. The

548 resolving power was set to 70,000 for ^{13}C labeling experiments. With retention times determined
549 by authenticated standards, resulting mass spectra and chromatograms were identified and
550 processed using MAVEN software⁴⁰. To obtain labeling information of cellular bicarbonate and
551 acetate, the labeling of carbamoyl group was obtained by comparing (i.e., computing the inverse
552 Cauchy product) citrulline to ornithine, and the labeling of acetyl group was obtained by comparing
553 N-acetyl-glutamate to glutamate.

554 **Substrate uptake and product secretion measurement**

555 For *Y. lipolytica*, 1 mL of culture was taken at each time point for media and cell dry weight (CDW)
556 analysis. The cells were centrifuged at 18,000 g for 10 min and the supernatant was subsequently
557 extracted, filtered (0.2 μm syringe filters), and analyzed on a high-performance liquid
558 chromatography (HPLC). The cell pellet was then wash once with 1 mL water to remove residual
559 media components and dried in a 60 °C oven until its mass remains unchanged. This mass was
560 taken to be the CDW per mL of culture. As for lipids, a small volume was extracted from the culture
561 such that it contains ~ 1 mg of CDW. The supernatant was discarded after centrifugation at 18,000g
562 for 10 min. 100 μL of an internal standard containing 2 mg/mL methyl tridecanoate (Sigma-
563 Aldrich) and 2 mg/mL glyceryl triheptadecanoate (Sigma-Aldrich) in hexane was added to each
564 sample. Transesterification was then carried out in 500 μL 0.5 N sodium methoxide solutions with
565 continuous vortexing at 1200 rpm for 60 min. Afterwards, 40 μL of 98% sulfuric acid was added to
566 neutralize the pH and 500 μL of hexane was used for extraction. Additional vortexing at 1200 rpm
567 for 30 min was carried out and centrifugation at 6,000 g for 1 min was performed to remove
568 cellular debris. The top hexane layer was used for analysis on a GC-FID system. All *Y. lipolytica*
569 specific rate data were normalized to the lipid-free CDW, which was the difference between the
570 measured CDW and the lipid titer.

571 For media analysis in *M. thermoacetica* cultures, small aliquots of the cultures were collected with
572 syringes inside the anaerobic glovebox over their exponential phase. Filtered media samples (0.2
573 μm syringe filters) were analyzed by YSI biochemistry analyzer for glucose and by HPLC for acetate
574 and formate along with other potential products (e.g., lactate and ethanol). Culture density was
575 measured by spectrophotometry (0.45 gCDW L⁻¹ OD₆₆₀⁻¹) at the time of sampling. The rates of
576 substrate uptake and product secretion were determined using the rates at which substrates,
577 products, culture density change over time. The carbon output rate for biomass was determined
578 using growth rate and elemental biomass composition of $\text{CH}_{2.08}\text{O}_{0.53}\text{N}_{0.24}$ ⁴¹. The net CO_2 fixation
579 rates were calculated based on the measured acetate and biomass carbon production rates less the
580 corresponding measured glucose carbon consumption rates. The fraction of electrons derived from
581 H_2 was inferred from the fraction of acetate and biomass carbons generated from net CO_2 fixation
582 since the average oxidation state of acetate and biomass carbons is nearly the same as that of
583 glucose.

584 For HPLC, 10 μL sample was injected into an Agilent 1200 High-Performance Liquid
585 Chromatography system coupled to a G1362 Refractive Index Detector (Agilent Technologies). A
586 Bio-Rad HPX-87H column was used for separation with 14 mM sulfuric acid as the mobile phase
587 flowing at 0.7 mL/min. For GC-FID, 1 μL of sample was injected at a split ratio of 50:1 into an
588 Agilent 7890B GC-FID system coupled to a J&W HP-INNOWax capillary column (Agilent

589 Technologies). The column was held at a constant temperature of 200 °C with helium as the carrier
590 gas (1.5 mL/min). The injection and FID temperatures were set to 260 °C.

591 **Headspace gas measurement**

592 After collecting the *M. thermoacetica* cultures from balch-type tubes inside the anaerobic glovebox
593 for intracellular and extracellular metabolite analysis, the empty balch-type tubes containing only
594 the headspace gas were stored at 4 °C until gas chromatography-mass spectrometry (GC-MS)
595 analysis. To measure CO₂ isotope labeling, 100 µl of headspace sample was collected from each tube
596 with a gastight syringe and injected in a multimode inlet, which was maintained at 180 °C, with a
597 split of 10. Samples were analyzed on a 7890A GC system with a 60 m GS-GasPro (0.320 mm
598 diameter) column coupled with a 5975C quadrupole mass spectrometer (Agilent). The oven was
599 kept at 90 °C for 3 minutes before heating to 260 °C at 45 °C/min and held at 260 °C for 1 minute.

600 **Flux balance analysis and isotope tracing flux analysis**

601 *M. thermoacetica* model based on the published genome-scale metabolic reconstruction⁴² was
602 employed for constraint-based flux analysis (see **Supplementary Information**). Among the
603 feasible metabolic flux distributions that satisfy steady-state mass balance and nutrient availability
604 constraints, optimal solutions that maximize/minimize objective functions were obtained using the
605 COBRA toolbox and a Gurobi solver⁴³. To determine CO₂ utilization capability, the objective was to
606 maximize CO₂ consumption, or equivalently, minimize CO₂ production. To determine the growth
607 potential using H₂ as the energy source, the objective was to maximize biomass production (i.e., cell
608 growth). Substrate uptake and product secretion rate constraints were selected based on
609 experimental or previously reported values.

610 To determine flux distributions, isotopomer mass balance constraints were also imposed based on
611 the ¹³C labeling results. For this purpose, the metabolic networks including glycolysis and PPP for *Y.*
612 *lipolytica* as well as lower glycolysis, the TCA cycle, anaplerosis, the reductive acetyl-CoA pathway
613 and the serine/glycine pathway for *M. thermoacetica* were constructed with carbon atom mapping.
614 The labeling of following metabolites were simulated by the elementary metabolite unit (EMU)
615 framework⁴⁴: for *Y. lipolytica*, G6P, F6P, 3PG, S7P, 6PG, R5P, PEP, and Pyr (**Supplementary Table**
616 **1**); for *M. thermoacetica*, 3PG, PEP, Ala, acetyl-CoA, Ser, Gly, Asp, Glu, and CO₂ (**Supplementary**
617 **Table 3**).

618 The flux distribution that best simulated the metabolite labeling and uptake-secretion rates was
619 found by minimizing the variance weighted-sum of squared residuals (SSR) between simulation
620 and experiment:

$$\min_v \sum \left(\frac{iso_{exp} - iso(v)}{s_{iso}} \right)^2 + \sum \left(\frac{v_{exp} - v}{s_v} \right)^2$$

621 v and $iso(v)$ denote in vector form the metabolic flux distribution and the simulated ¹³C labeling of
622 metabolites as a function of v . v_{exp} and iso_{exp} denote measured fluxes and measured metabolite
623 labeling; s_v and s_{iso} , their measurement standard deviation. The 95% confidence interval for each
624 best fit flux was obtained by searching for the minimum and maximum flux values that increase the
625 minimum SSR by less than the χ^2 cutoff (1 degree of freedom) of 3.84.⁴⁵

626 **Code availability**

627 The code for metabolic flux and free energy analysis is available on the GitHub public repository:
628 https://github.com/jopark/moorella_yarrowia

629

630 **References**

- 631 37 Tai, M. & Stephanopoulos, G. Engineering the push and pull of lipid biosynthesis in
632 oleaginous yeast *Yarrowia lipolytica* for biofuel production. *Metab Eng* **15**, 1-9,
633 doi:10.1016/j.ymben.2012.08.007 (2013).
- 634 38 Michaelis, L. & Barron, E. S. G. Oxidation-reduction systems of biological significance.
635 II. Reducing effect of cysteine induced by free metals. *J Biol Chem* **81**, 29-40 (1929).
- 636 39 Rabinowitz, J. D. & Kimball, E. Acidic acetonitrile for cellular metabolome extraction
637 from *Escherichia coli*. *Anal Chem* **79**, 6167-6173, doi:Doi 10.1021/Ac070470c (2007).
- 638 40 Clasquin, M. F., Melamud, E. & Rabinowitz, J. D. LC-MS data processing with
639 MAVEN: a metabolomic analysis and visualization engine. *Current protocols in*
640 *bioinformatics / editorial board, Andreas D. Baxevanis ... [et al.] Chapter 14*, Unit14 11,
641 doi:10.1002/0471250953.bi1411s37 (2012).
- 642 41 Tracy, B. P., Jones, S. W., Fast, A. G., Indurthi, D. C. & Papoutsakis, E. T. Clostridia: the
643 importance of their exceptional substrate and metabolite diversity for biofuel and
644 biorefinery applications. *Curr Opin Biotech* **23**, 364-381,
645 doi:10.1016/j.copbio.2011.10.008 (2012).
- 646 42 Islam, M. A., Zengler, K., Edwards, E. A., Mahadevan, R. & Stephanopoulos, G.
647 Investigating *Moorella thermoacetica* metabolism with a genome-scale constraint-based
648 metabolic model. *Integr Biol (Camb)* **7**, 869-882, doi:10.1039/c5ib00095e (2015).
- 649 43 Schellenberger, J. *et al.* Quantitative prediction of cellular metabolism with constraint-
650 based models: the COBRA Toolbox v2.0. *Nat Protoc* **6**, 1290-1307,
651 doi:10.1038/nprot.2011.308 (2011).
- 652 44 Antoniewicz, M. R., Kelleher, J. K. & Stephanopoulos, G. Elementary metabolite units
653 (EMU): A novel framework for modeling isotopic distributions. *Metab Eng* **9**, 68-86,
654 doi:Doi 10.1016/J.Ymben.2006.09.001 (2007).
- 655 45 Antoniewicz, M. R., Kelleher, J. K. & Stephanopoulos, G. Determination of confidence
656 intervals of metabolic fluxes estimated from stable isotope measurements. *Metab Eng* **8**,
657 324-337, doi:Doi 10.1016/J.Ymben.2006.01.004 (2006).

658